



Measuring the Electrical Status of the Bionic Ear. Re-thinking the Impedance in Cochlear Implants

Federico A. Di Lella^{1*}, Matias Parreño¹, Florencia Fernandez¹, Carlos M. Boccio^{1†} and Sebastián A. Ausili^{2*†}

¹ Department of Otolaryngology, Hospital Italiano, Buenos Aires, Argentina, ² Department of Otolaryngology, University of Miami, Miami, FL, United States

OPEN ACCESS

Edited by:

Antonio Lanatà,
University of Florence, Italy

Reviewed by:

Xin Liu,
University of California, San Diego,
United States
Salvatore Andrea Pullano,
University Magna Graecia
of Catanzaro, Italy

*Correspondence:

Federico A. Di Lella
federico.dilella@hospitalitaliano.org.ar
Sebastián A. Ausili
s.ausili@miami.edu

[†] These authors share senior
authorship

Specialty section:

This article was submitted to
Bionics and Biomimetics,
a section of the journal
Frontiers in Bioengineering and
Biotechnology

Received: 01 June 2020

Accepted: 26 August 2020

Published: 18 September 2020

Citation:

Di Lella FA, Parreño M,
Fernandez F, Boccio CM and Ausili SA
(2020) Measuring the Electrical Status
of the Bionic Ear. Re-thinking
the Impedance in Cochlear Implants.
Front. Bioeng. Biotechnol. 8:568690.
doi: 10.3389/fbioe.2020.568690

As in any biophysical electrode-tissue environment, impedance measurement shows a complex relationship which reflects the electrical characteristics of the medium. In cochlear implants (CIs), which is mostly a stimulation-oriented device, the actual clinical approach only considers one arbitrary time-measure of the impedance. However, to determine the main electrical properties of the cochlear medium, the overall impedance and its subcomponents (i.e., access resistance and polarization impedance) should be described. We here characterized, validated and discussed a novel method to calculate impedance subcomponents based on CI measurement capabilities. With an electronic circuit of the cochlear electrode-tissue interface and its computational simulation, the access resistance and polarization impedance were modeled. Values of each electrical component were estimated through a custom-made pulse delivery routine and the acquisition of multiple data points. Using CI hardware, results fell within the electronic components nominal errors ($\pm 10\%$). Considering the method's accuracy and reliability, it is readily available to be applied in research-clinical use. In the man-machine nature of the CI, this represents the basis to optimize the communication between a CI electrode and the spiral ganglion cells.

Keywords: cochlear implants, electrical stimulation, electrical impedance, impedance subcomponents, voltage telemetry

INTRODUCTION

A cochlear implant (CI), also known as “the bionic ear,” is a medical electronic prosthesis that can be precisely controlled to stimulate the auditory nerve and restore the hearing sense. The evaluation of CI functioning is facilitated by various analysis tools, one of the most important is the electric impedance measurement. While it is impossible to directly assess impedance, its values can be obtained by measuring voltage, as provided by Ohm's law. In CIs, this measurement is performed by using a protocol known as “voltage telemetry” (Hughes, 2013; Wolfe, 2017).

To obtain the electric potential difference at a certain point in time, the CI sends a constant current iso-biphasic pulse and retrieves the measured voltage (French, 1999; von Rohr, 2011). This metric provides important clinical information about the device and individual electrode function, in both intra and post-operative patient's appointments. In today's CI standard of care, it is mainly used to investigate the electrode's overall function (Paasche et al., 2006), detect problems such as short-circuit or open circuit (Goehring et al., 2013), guide audio-processors

fitting (Khater et al., 2015), and determine power consumption (Newbold et al., 2015). For example, intra-operatively this measure checks the integrity of the device after surgical manipulation. Post-operatively is also performed at the beginning of every CI-fitting appointment, establishing the compliance range for the electrical stimulation of the auditory nerve.

The interface between the CI electrode and the spiral ganglion cells is critical for the transmission of information via electro-neural stimulation and consequently, a crucial research area in which improvements can be made (Saunders et al., 2002). According to several authors, the impedance reflects the electrical status of the complex electrode-tissue relationship (Ni et al., 1992; Hughes et al., 2001; Tykocinski et al., 2005). However, the actual clinical impedance measurement provides very limited information to that end, as it was developed for a different purpose. The clinical approach is based on a single voltage measurement and the predefined settings (i.e., voltage evaluation) significantly differ along CI manufacturers (Hughes, 2013; Wolfe, 2017). This makes the actual approach not specifically useful to explore the characteristics of the electro-tissue interface. A complete understanding of the impedance and its subcomponents could provide insights of the actual endocochlear nature around the electrode, extending its use beyond the actual clinical implementation.

Voltage response measurement and impedance subcomponents calculations were reported *in vitro* (Newbold et al., 2004, 2010; Giardina et al., 2018), in animal models (Smith and Finley, 1997; Tykocinski et al., 2001; Newbold et al., 2014) and in humans (Tykocinski et al., 2005; Newbold et al., 2014; Di Lella et al., 2019). Smith and Finley (1997) described the influence of the electrode configuration and electrical stimulation in the complex interface between electrode and neural target in cats. Based on the same animal model, Tykocinski et al. (2001) described the two components of the total impedance, the access resistance and the polarization impedance. Later, Newbold et al. (2014) reported a stimulus-induced reduction in impedance. More recently, Giardina et al. (2018) measured impedance subcomponents *in vitro* using Advanced Bionics, Ltd. hardware. Furthermore, Di Lella et al. (2019) described impedance subcomponent calculation *in vivo* based on voltage telemetry using Cochlear, Ltd. CIs. However, despite the existing literature, methodological details, specific setup configurations and measurement validation are lacking, which restrain these measurements in the clinical setting.

Our study is an extension of the work done by Di Lella et al. (2019) where the impedance subcomponents in cochlear implant users were measured. This study describes the method in detail to recreate the complex morphology of the voltage response for Cochlear, Ltd. devices. This is based completely – and solely – on the CI hardware, without requiring external elements. Unlike actual clinical impedance measures, we extract the impedance subcomponents for a better description of the electrode-tissue relationship. Moreover, we evaluate the accuracy of the subcomponent assessment of the method employing computational circuit simulation and *in silico* electronic hardware. By providing this characterization, our method is not only better supported

but, more importantly, translationally ready to be applied in real CI users.

MATERIALS AND METHODS

Modeling the Electrode-Tissue Interface

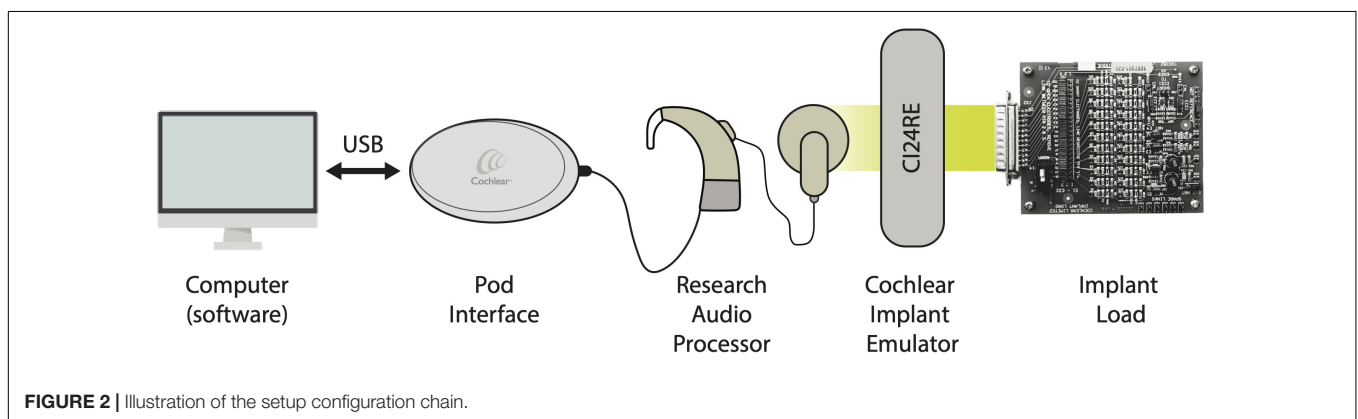
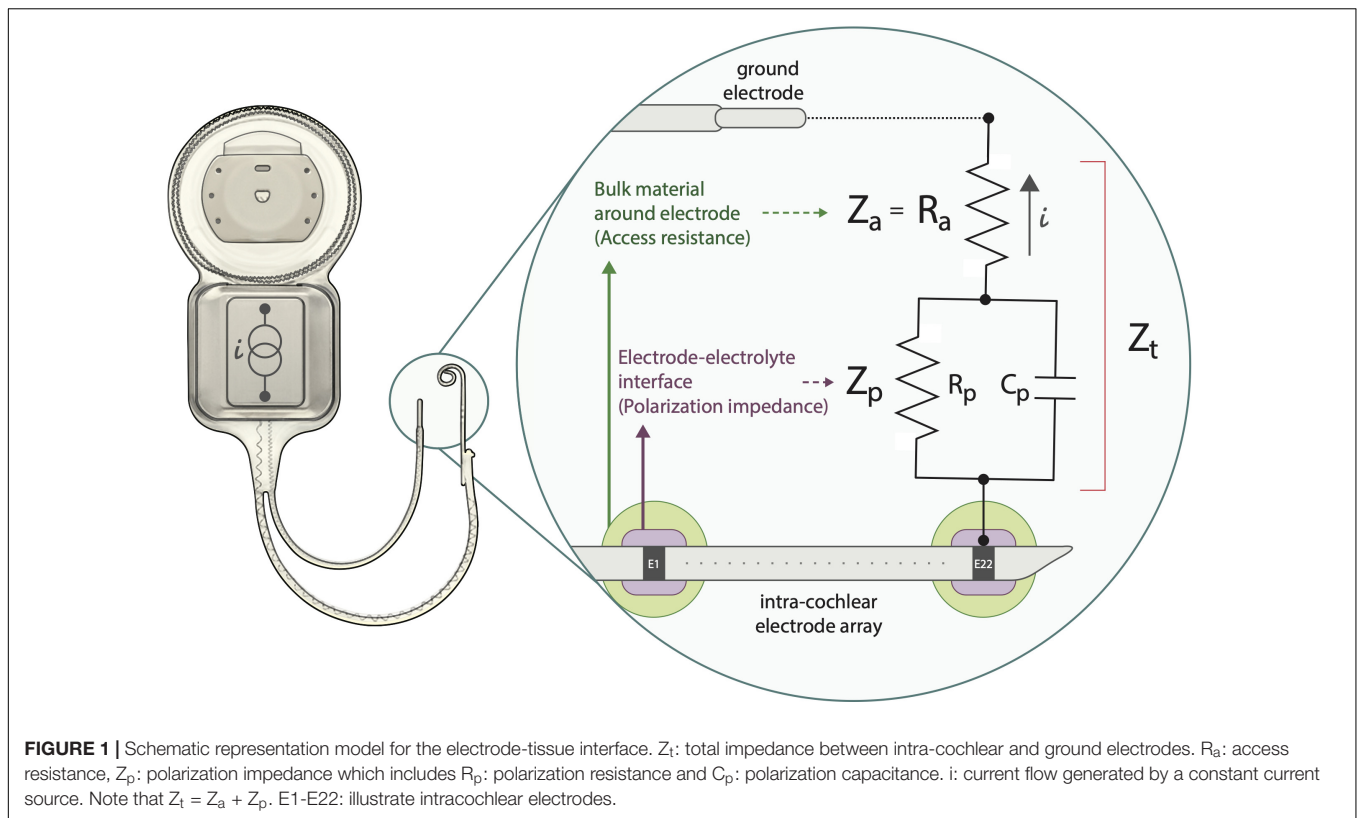
The electrical medium characteristics of the electrode-tissue interface in the inner ear can be modeled with an equivalent electrical circuit (Vanpoucke F. et al., 2004; Vanpoucke F.J. et al., 2004; Tykocinski et al., 2005; Newbold et al., 2010; Mesnildrey et al., 2019). The standard model of a biopotential electrode used for the transduction of ionic current into electric current (both for stimulation and recording) closely recreates the electrical behavior of the electrode-tissue interface in the cochlea. This model facilitates its understanding and makes the model's equations accessible. In this study, we adopted an existing model where the overall impedance Z_t includes an access impedance Z_a and a polarization impedance Z_p , being $Z_t = Z_a + Z_p$ (**Figure 1**) (Vanpoucke F. et al., 2004; Tykocinski et al., 2005; Newbold et al., 2010). Briefly, an access resistance (R_a) is in series with a parallel capacitor (C_p) and a resistor (R_p). Physiologically, R_a represents the bulk surrounding tissue around the electrode inside the cochlea, including fibrous tissue and new bone growth. The sub-component Z_p (R_p and C_p) arises from the narrow layer on the surface of the electrode, the electrode-electrolyte interface. C_p models the behavior at the electrolyte interface, while the faradaic resistance R_p is associated with the transition from electrical to ionic charge carriers. As a whole, Z_p is considered a consequence of electrochemical effects, including deposits of electrically charged proteins that modify its distribution with electrical stimulation (Tykocinski et al., 2005).

Setup Configuration

An illustration of the overall setup chain is depicted in **Figure 2**. In detail, a custom-made software was designed specifically to perform the measurements and obtain the data. Delphi® (Embarcadero, Inc., Austin, TX, United States) programming language together with the dynamic link libraries (DLLs) provided by Cochlear, Ltd. were implemented to communicate with the Nucleus Interphase Communicator (NIC). This software was compiled to run under the Microsoft Windows operating system (Windows 7® and later).

A Cochlear Freedom Speech processor (research firmware ver. 0102E00F02) was connected to the Programming Pod Interface, providing the input to the CI (CI24RE) emulator. The implant load (IL) was coupled to the electrode's terminals of the implant emulator (via a 25-way D connector) and served as a cochlea simulator to measure and compute the impedances. Each *in silico* electrode routing in the IL is defined by the circuit shown in **Figure 1** (a R_a in series with a parallel C_p and R_p).

For the purpose of validation, two different ILs were implemented. For the clinical approach validation, we measured the IL provided by Cochlear, Ltd. In this circuit R_a varies from 3 to 10 k Ω along electrodes 1 to 22, respectively, and Z_p remains constant ($C_p = 100$ nF and $R_p = 1$ M Ω). For the validation of the subcomponents R_a and C_p we employed a custom IL hardware.



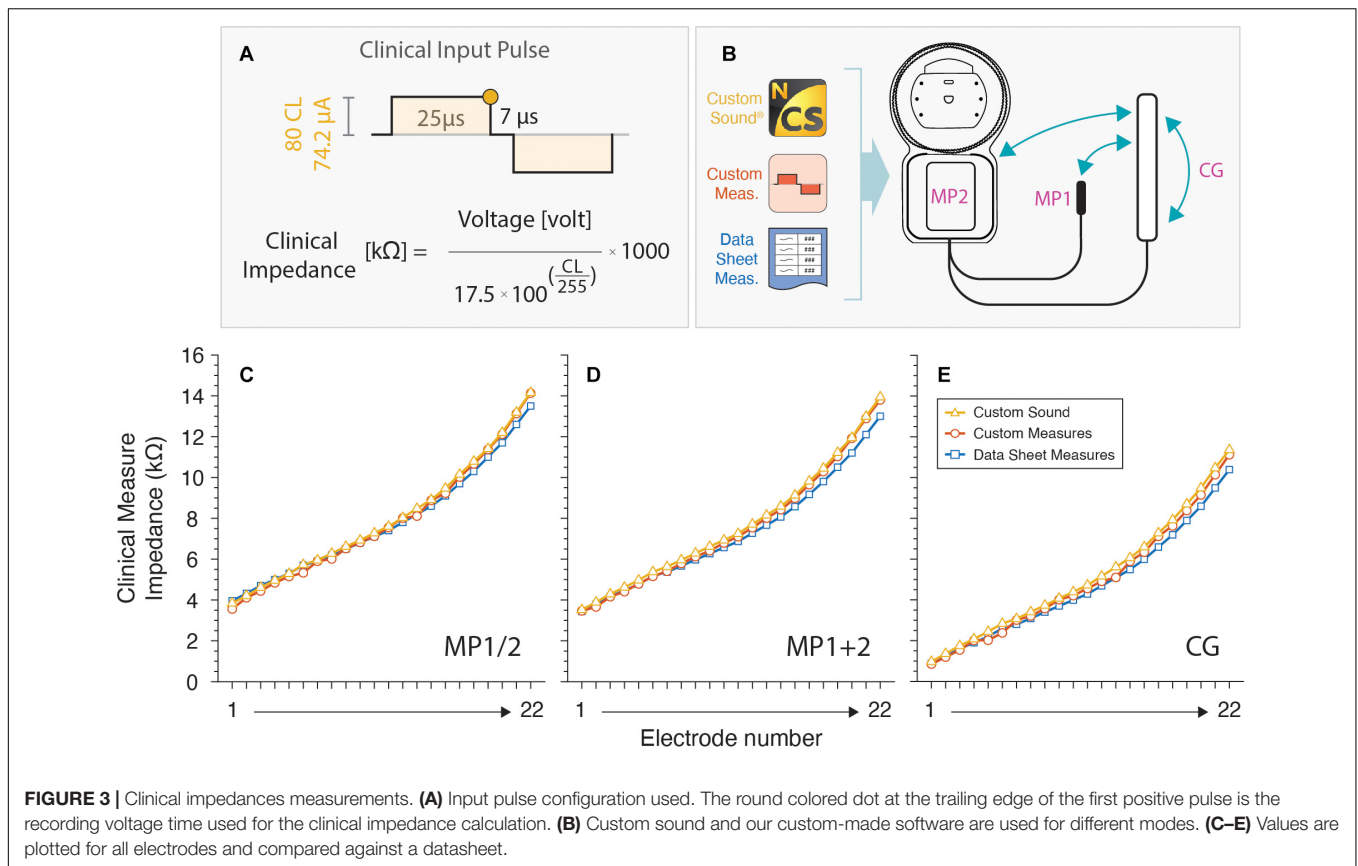
Its design allows to fix R_a while varying C_p (R_a validation) and vice versa (C_p validation). The subcomponent R_a varied from 3 to 9.3 k Ω , C_p ranged between 2.8 and 54 nF and $R_p = 1$ M Ω . All electronic components have a tolerance of $\pm 10\%$. In order to work in a relevant range, the selected nominal values included the reported of *in vivo* studies (Tykocinski et al., 2005; Di Lella et al., 2019; Mesnildrey et al., 2019). In all cases, the presented voltage value is an average of four consecutive measures. Due to the negligible variation in the measures (± 0.001 V), figures only depict the mean voltage value.

We also replicated the custom ILs with virtual computational circuits in MATLAB Simulink (MathWorks, Natick, MA, United States). The input pulses were driven by a current source and the same subcomponents were modeled. The complete

waveform was retrieved from the virtual simulation and verified with our fitting on real measurements.

Clinical Impedance Measurement

To validate the accuracy of our measure, we replicated the clinical voltage telemetry. For that purpose, Cochlear, Ltd. clinical software and IL data sheet were contrasted to our measures. Overall impedances (Z_t) were obtained with Cochlear Custom Sound Suite™ (version 5.2). In this software the input biphasic pulse is predefined by the manufacturer with 80 current level (CL) (or 74.2 μ A), 25 μ s of pulse width (PW) and interphase gap (IPG) of 7 μ s (Figure 3A; Hughes, 2013; Wolfe, 2017; Cochlear Limited, 2019). The recording time used for this clinical Z_t is also predefined to be at



the trailing edge of the positive pulse-phase. The equation in **Figure 3A** shows the Ohm's law equation for the clinical impedance calculation. Here, the numerator is the measured voltage (in volt) at 25 μ s and the denominator the analytical conversion from CL to microamperes (according to Cochlear, Ltd.). Note that the fraction is multiplied by 1000 to represent the result in $k\Omega$. To strengthen the validation measure, we also compare impedances varying stimulation modes (**Figure 3B**): monopolar MP1, monopolar MP2, monopolar MP1+2, and common ground (CG).

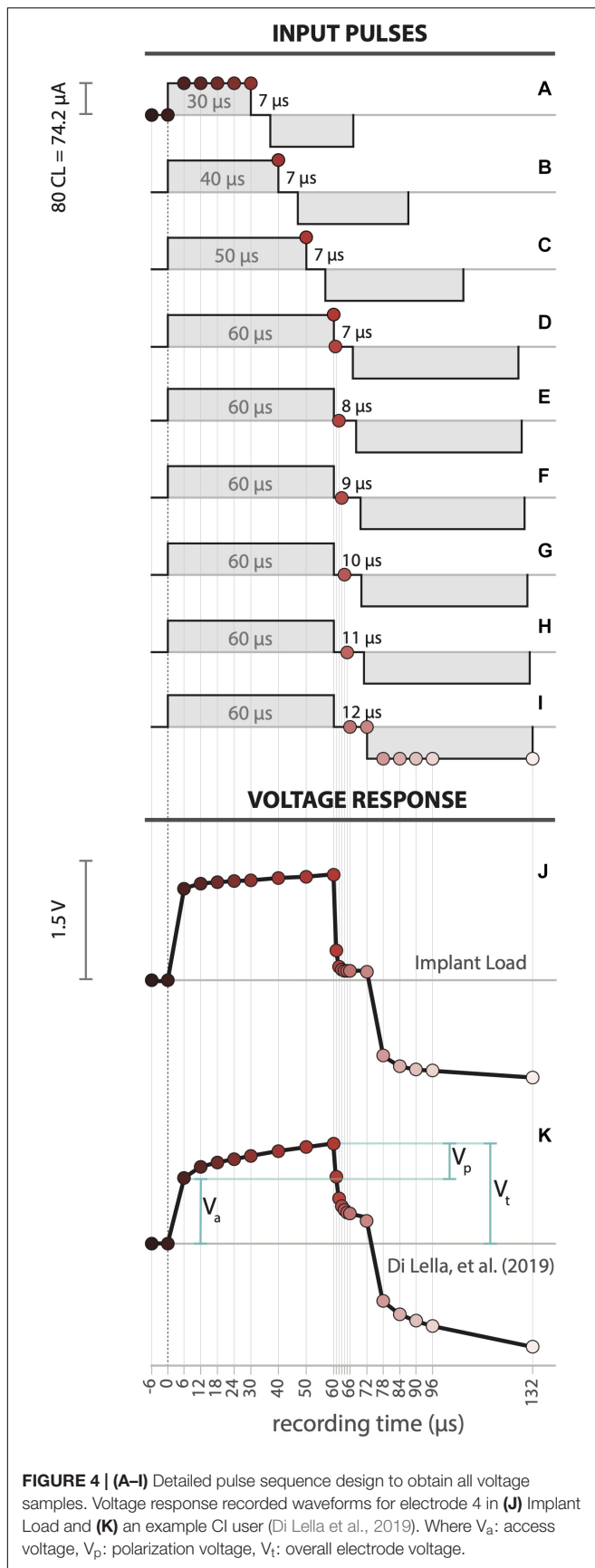
Stimulation Pulses Parameters and Voltage Response Wave

The latest Cochlear, Ltd. CI chipset (CIC4) allows up to 14 voltage measurements in different time points for a given pulse. Some of those time points are fixed by hardware, but others depend on the PW and IPG. Therefore, to acquire more points and reconstruct the voltage morphology, several biphasic pulses were used (**Figure 4**). To obtain the negative-lead voltages, a polarity change was applied. The positive to negative transition is determined at the beginning of the negative phase of stimulus. Note that, although the complete waveform was reconstructed, only voltages from the positive pulse-phase were used to calculate impedance subcomponents.

Under electrical hearing, pulse parameters limits are governed by sound perception thresholds and hearing discomfort.

This depends on the pulse's overall energy and is directly related to both the PW and CL. However, voltage telemetry can be achieved without sound perception, making this measurement convenient and simple for the CI user. Low current pulses with 100 CL and 25 μ s are inaudible for most but not all CI recipients (Wolfe and Schafer, 2014). Based on our preliminary experience, CL below 100 units and longer PW around 50 μ s do not produce sound perception. Moreover, the built-in analog to digital (AD) amplifier of the CI has limited resolution (0 to 10 volt @16 bit) defining minimum parameters for proper sensitive measures. The pulse current level was set at 80 (74.21 μ A) and PW and IPG were modified sequentially to accommodate between sub-threshold sound perception and voltage wave resolution. Points 1 to 7 were collected using pulses with 30 μ s PW and 7 μ s IPG (**Figure 4A**). Points 8 to 11 were measured using pulses with increasing PW length, from 40 to 60 μ s in steps of 10 μ s with a fixed 7 μ s IPG (**Figures 4B–D**). For the subsequent measures the PW was fixed to 60 μ s and varied the IPG. For points 12 to 16, we recorded with IPG that increases from 7 to 12 μ s in 1 μ s steps (**Figures 4E–I**). Last, points 17 to 22 were determined by using 12 μ s IPG (**Figure 4I**).

A total of 22 voltage points (**Figures 4J,K**) are extracted from the pulse sequence previously described. This experimental design allows the recreation of the voltage waveform covering -6 to 132 μ s. The overall morphology shows a clear consistency with the proposed model (Tykocinski et al., 2005). The abrupt rise in the voltage at the onset of the current pulse corresponds



to the resistive component of the circuit (access voltage, V_a). This is followed by a slowly rising voltage limb, which represents the capacitive component (polarization voltage, V_p). The overall electrode voltage is the sum of these values ($V_t = V_a + V_p$).

Calculation of Access Resistance and Polarization Impedance

Impedance can be studied using a phasor transform or in the time domain. The phasor transform is represented by a real (resistive) and an imaginary (reactive) components and is not a function of time. By the study of the time variant voltage waveform morphology of a resistor-capacitor circuit, it is possible to approximate the magnitudes of its subcomponents. We here used the time domain approach, also described in Tykocinski et al. (2005) and Giardina et al. (2018).

From the adopted electrical model, the relation between the overall impedance (Z_t), access resistance (R_a) and polarization impedance (Z_p) are well-known and can be mathematically described as follow:

$$Z_t(t) = Z_a + Z_p(t) \quad (1)$$

with

$$Z_a = \frac{V_a}{i} = R_a \quad (2)$$

$$Z_p(t) = \frac{V_p(t)}{i} = R_p \cdot \left(1 - e^{-\frac{t}{R_p \cdot C_p}}\right) \quad (3)$$

The access resistance (R_a) is simply the quotient of the measured access voltage (V_a ; **Figure 4K**) with the current pulse amplitude (Eq. 2). Unlike R_a , Z_p varies over time. Therefore, the total impedance can be determined as:

$$Z_t(t) = R_a + R_p \cdot \left(1 - e^{-\frac{t}{R_p \cdot C_p}}\right) \quad (4)$$

We fitted Eq. 4 to our data points with R_p and C_p as free parameters. This was achieved by minimizing the sum-squared deviation using iterative least squares estimation in MATLAB (MathWorks, Natick, MA, United States). The effect of the access resistance (R_a) on the voltage waveform is instantaneous once the pulse is delivered. However, due to the hardware limitations we can only record with a 6 μ s offset. Therefore, we estimated R_a at 0 μ s by an extrapolation of the fitting.

RESULTS

Clinical Impedance

To validate our measurement tool, we compared the results of the Custom Sound with our custom-made software. Results were also verified with provided values by Cochlear, Ltd. IL data sheet. Results are depicted for MP1 and MP2 (**Figure 3C**), MP1+2 (**Figure 3D**), and CG (**Figure 3E**) coupling modes.

Impedance curves are practically overlapped showing negligible errors along IL electrodes. This comparison serves as a strong validation for the design of our custom measurement tool.

Complete Voltage Response Wave

Full voltage response wave was obtained for each electrode of the IL in MP1 coupling mode (see **Figure 3B**). The IL voltage waveform (**Figure 4J**) showed a significant similarity with a real CI user measurement (**Figure 4K**) Di Lella et al. (2019). Moreover, both curves relate to the pattern of the modeled electrical circuit (see **Figure 1**). The described pulse transmission and voltage telemetry acquisitions were completed in approximately 1 min for all electrodes.

Impedance Subcomponents

Theoretical Analysis

For a better understanding of the subcomponents and its relationship with Z_t , we varied R_a , C_p and R_p in Eq. 4 and analyzed its results. This was modeled for 6 to 60 μs range, which is the main region for subcomponents calculation. The main two components that play a major role modifying the Z_t curve are R_a and C_p as it's illustrated in **Figure 5A**. First, we varied R_a between 3 and 10 $\text{k}\Omega$ while maintaining $R_p = 1 \text{ M}\Omega$ and $C_p = 10 \text{ nF}$ (**Figure 5B**). R_a linearly modifies the abrupt rise of Z_t at its onset. As R_a increases higher Z_t offsets are seen. Secondly, we ranged $2 \text{ nF} \leq C_p \leq 10 \text{ nF}$ with $R_a = 3 \text{ k}\Omega$ and $R_p = 1 \text{ M}\Omega$ (**Figure 5C**). We observed that C_p strongly affects the slope of the slowly rising polarization component limb with an inverse relation. Finally, we used $R_a = 3 \text{ k}\Omega$ and $C_p = 10 \text{ nF}$ while varying $100 \text{ k}\Omega \leq R_p \leq 1000 \text{ k}\Omega$ (**Figure 5D**). Despite the large R_p variation there was negligible modification on Z_t , showing no overall impact. Therefore, we excluded R_p from the subcomponent analysis due to its small variation and very poor informative use. Note, however, that this does not affect the estimation of the other circuit elements (Mesnildrey et al., 2019). Moreover, *in vitro* CI measurements also yielded an extremely high estimation for R_p ($>10^{15} \Omega$; Mesnildrey et al., 2019) suggesting that no current passes through this resistor. This effect is intrinsically related to the metal-electrolyte interface, meaning that the kinetics of the

dissolution of the platinum electrode into the electrolyte is extremely slow (Wieckowski, 1999).

Experimental Analysis

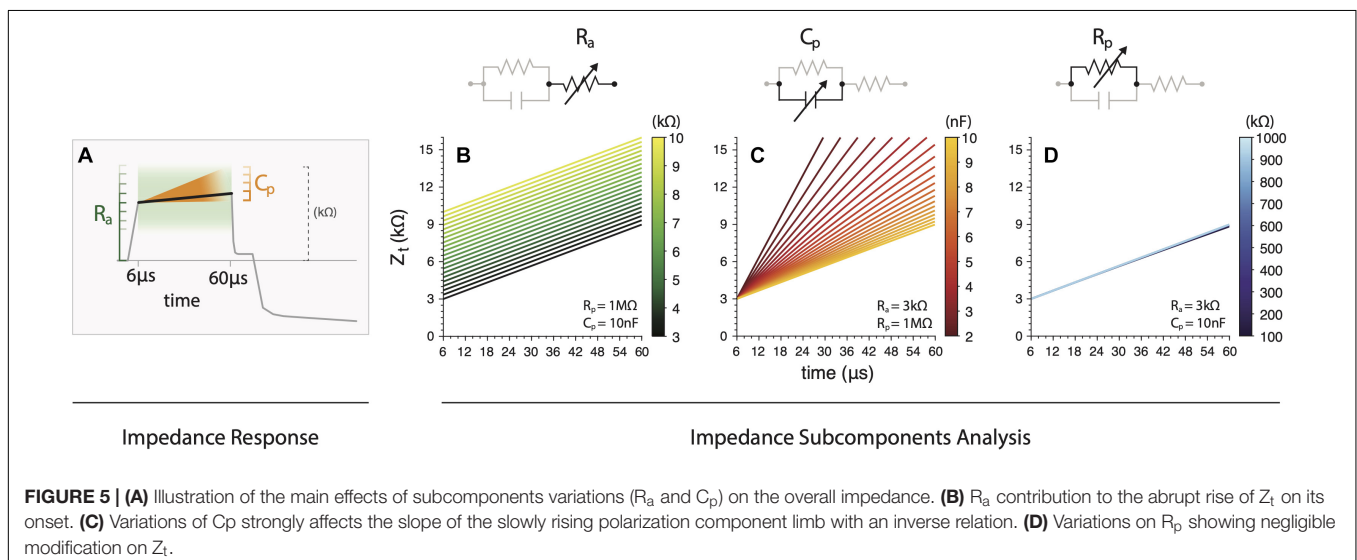
Based on this previous theoretical analysis, R_a and C_p were inferred for all electrodes from the custom IL. Our method outcomes were contrasted with the corresponding electrical hardware and virtual circuit simulation values (**Figure 6**). To measure isolated values of R_a and C_p ensuring its correct validation, we first fixed C_p and R_p while varying only R_a (**Figure 6A**) and then fixed R_a and R_p varying C_p (**Figure 6E**). Examples of raw measured data and their corresponding Z_t fitting are depicted in **Figures 6B,F**.

Overall, our analysis showed high accuracy for R_a as well as C_p subcomponents. All measures have small errors and fall within the electrical component's tolerance range in most cases. We did observe small drops in C_p values for higher electrodes (**Figure 6D**) and in R_a for the first electrodes (**Figure 6G**) when those subcomponents are fixed. This effect was only observed for the combination of R_a and C_p that yields high Z_t (higher clinical values than usual (Hughes, 2013)). These drops were not observed when fitting the theoretical simulated circuits.

DISCUSSION

A Novel Method

To the author's knowledge, this is the first report with a complete description, analysis and validation of the electrical CI impedance's subcomponents measurement for standard Cochlear, Ltd. devices. This protocol ensures that all parameters are measured only using the CI, making it readily available for clinical research purposes. We also ensured that all measures include the known impedance values measured in real CI users. As impedance subcomponents are related with the electrode-tissue interface, they can be exploited to improve CI stimulation. In the man-machine nature of the CI, this represents



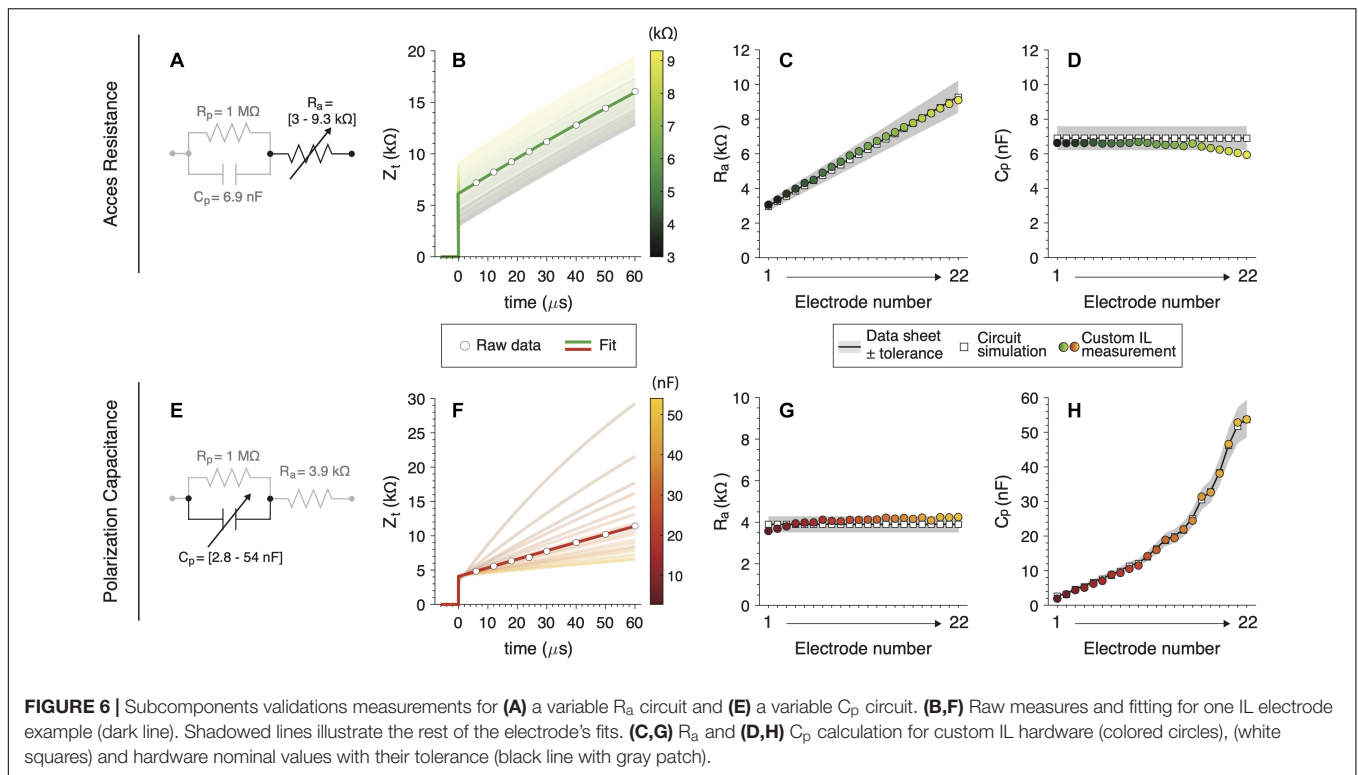


FIGURE 6 | Subcomponents validations measurements for (A) a variable R_a circuit and (E) a variable C_p circuit. (B,F) Raw measures and fitting for one IL electrode example (dark line). Shadowed lines illustrate the rest of the electrode's fits. (C,G) R_a and (D,H) C_p calculation for custom IL hardware (colored circles), (white squares) and hardware nominal values with their tolerance (black line with gray patch).

the basis to optimize the communication between a CI electrode and the spiral ganglion cells.

In electrical circuits, the impedance is normally assessed with the support of an external access tool, where a continuous voltage recording provides high measurement resolution. Since direct intracochlear electrodes measurement is not plausible *in vivo*, we elaborated a novel technique only based on the CI hardware capabilities. We demonstrated that a high resolution and accuracy can be achieved via the CI telemetry communication protocol. In other words, we 'reversed-engineer' the *in silico* black-box, which gives us the opportunity to similarly 'unblind' the electrical characteristics of the electrode-tissue interface within the implanted inner ear.

The adopted electrical electrode-tissue interface model (Tykocinski et al., 2005) showed high correlation between its theoretical electrical behavior and our test-bench results. We also highlight the most important subcomponents to be considered for future analysis (i.e., R_a and C_p), due to the negligible variation of Z_t over a wide range of R_p (Figure 5C). Thus, we observe that the electrical electrode-tissue interface is mostly driven by R_a and C_p , making these subcomponents the most relevant variables. Other modified models have been proposed to describe the electrical behavior of this interface (e.g., Duan et al., 2004; Franks et al., 2005; Mesnildrey et al., 2019). Usually, accurate biophysical predictions involve complex representations with a high number of elements in the modeling framework. However, note that even with the simplified model adopted in this study, we observed similar voltage waveforms between *in vivo* (Di Lella et al., 2019) and *in silico* (see Figures 4J,K). Furthermore, since this simple model is mathematically very

well-described, calculations of each circuit subcomponent can be quickly achieved.

Moreover, our custom design software successfully measures and processes impedance subcomponents. The novel approach here described is ready to be implemented in CI users as it is (as also demonstrated in Di Lella et al., 2019), making this approach readily useful for future applied research in CI users. This study also serves as a validation document given the presented evidence and proven correlation between objective measures, real electronic components in IL models, and virtual circuit simulations.

Toward a Real Clinical Use

The current clinical CI-software measure impedances with a predefined (and almost arbitrary selected) series of parameters. Only one biphasic pulse is used as input (e.g., see Figure 3A for Cochlear, Ltd.) and a single voltage data point is measured from the complex voltage electrode-tissue response. Through ohm's law, the retrieved voltage (V_t) is converted into impedance (Z_t) and shown on the clinical software. However, the variable Z_t is determined by the main following variables:

- **Measurement Time.** As determined in Eq. 4, the capacitive component of the polarization impedance (Z_p) generates an asymptotic growing curve. Therefore, Z_t systematically changes from Z_a to $Z_a + Z_p$.
- **Coupling Mode.** The configuration of where the circuit's ground is set modulates the overall measure of Z_t . This was also observed in our custom software validation (Figures 3C-E).

- **Electrode design.** The electrode surface dimensions (i.e., area of the physical platinum electrode) also impacts and contributes to Z_t . For example, with smaller electrode surfaces, higher Z_t values are expected (Hughes, 2013).
- **Input biphasic pulse.** As Z_t increases over time, the shorter the input PW, the smaller the Z_t captured (and vice versa).

Impedance subcomponent calculations require precise measurement capabilities. This is directly affected by the following CI-related issues:

- **CI hardware-related issues.** In all measurement oriented devices the internal circuitry defines the intrinsic error and uncertainty of its measure (Horowitz and Hill, 2015). This is of importance in CI devices, which are not specifically designed to perform very precise measures. In our results, C_p (electrodes > 17, **Figure 6D**) and R_a (electrodes < 4, **Figure 6G**) showed a measurement offset which we attributed to CI hardware limitations. This effect was not observed in our virtual circuit simulation fitting. More research should be done to describe the range of Z_t to compute impedance subcomponents through the measurement capabilities of the CI.
- **CI software-related issues.** The CI software platform controls and defines the voltage measurement protocol. For example, Cochlear, Ltd. programming library tool only retrieves one voltage measure per pulse. This forces to employ a pulse sequence routine (see **Figures 4A–I**) which modulates the electrode-electrolyte characteristics, Z_p (Newbold et al., 2014). Moreover, the implemented software tools do not allow to perform voltage measures from pulse onset to 6 μ s. This clearly introduces a measurement offset in R_a .

As here discussed, this measure involves device-related variables that are not related to the patient's specific clinical status. Therefore, the so-called "clinical" impedance is far from being a representative clinical measure. The only useful interpretation of this value is when compared within the subject's measurement (e.g., over time), only if no internal change of components was done.

CI technology brings the unique possibility to assess the relation between the electrode and the endo-cochlear medium by providing intra-cochlear measurements. Obviously, the medium properties are independent of the utilized device. Our analysis focuses on the impedance subcomponents (R_a and C_p), which, unlike Z_t , are independent of device-related issues. In other words, by adopting the proposed procedure it is possible to associate the impedance to an effective clinical and useful measure.

REFERENCES

Cochlear Limited (2019). *Custom Sound EP software Version 5.2 User Guide D1418673 ISS4*, 86.

The adoption of impedance subcomponents is a promising field to better assess the implanted cochlear health. At present, one of its clinical implementations was oriented to report changes in the cochlear medium after implantation (Tykocinski et al., 2005; Di Lella et al., 2019). Future electrode's design can be based on the electrode-tissue relationship and the stimulation protocol might be optimized according to certain endo-cochlear properties. Moreover, this approach can precisely monitor the impact of drug-releasing electrodes as well as surgical approaches for its insertion. Longitudinal studies with this tool will not only shed some light to a better understanding of the inflammatory response in the implanted inner ear, but also the development of new approaches to enhance CI-hearing performance. Only increasing the knowledge about the living electrical medium between the electrode and the neurons in the cochlea, CI outcomes can be improved.

CONCLUSION

This is the first report with a complete and detailed description, analysis and validation of the electrical impedance subcomponents measurement for Cochlear, Ltd. CIs. This was assessed solely through the CI capabilities, which makes it directly available for clinical research purposes. Even though the present method is based on a simplified model of the electrode-tissue electrical interface, *in silico* values were obtained with high accuracy. In conclusion, based on a better description of this human-machine interface, this approach may enhance CI-hearing performance in our implanted patients.

DATA AVAILABILITY STATEMENT

The raw data supporting the conclusions of this article will be made available by the authors, without undue reservation.

AUTHOR CONTRIBUTIONS

FD and SA designed the methodological approach, collected the data, performed the data analysis, and wrote the manuscript. MP and FF supported the data collection and provided critical revision of the manuscript. CB supervised the findings and revised final manuscript. All authors contributed to the article and approved the submitted version.

ACKNOWLEDGMENTS

Equipment was provided by Cochlear, Ltd.

Di Lella, F. A., De Marco, D., Fernández, F., Parreño, M., and Boccio, C. M. (2019). In vivo real-time remote cochlear implant capacitive impedance measurements: a glimpse into the implanted inner ear. *Otol. Neurotol.* 40(Suppl. 1), S18–S22.

- Duan, Y. Y., Clark, M. M., and Cowan, R. S. C. (2004). A study of intra-cochlear electrodes and tissue interface by electrochemical impedance methods in vivo. *Biomaterials* 25, 3813–3828. doi: 10.1016/j.biomaterials.2003.09.107
- Franks, W., Schenker, I., Schmutz, P., and Hierlemann, A. (2005). Impedance characterization and modeling of electrodes for biomedical applications. *IEEE Trans. Biomed. Eng.* 52, 1295–1302. doi: 10.1109/tbme.2005.847523
- French, M. L. (1999). Electrical impedance measurements with the CI24M cochlear implant for a child with *Mondini dysplasia*. *Br. J. Audiol.* 33, 61–66. doi: 10.3109/03005364000000100
- Giardina, C. K., Krause, E. S., Koka, K., and Fitzpatrick, D. C. (2018). Impedance measures during in vitro cochlear implantation predict array positioning. *IEEE Trans. Biomed. Eng.* 65, 327–335. doi: 10.1109/tbme.2017.2764881
- Goehring, J. L., Hughes, M. L., Baudhuin, J. L., and Lusk, R. P. (2013). How well do cochlear implant intraoperative impedance measures predict postoperative electrode function? *Otol. Neurotol.* 34, 239–244. doi: 10.1097/mao.0b013e31827c9d71
- Horowitz, P., and Hill, W. (2015). *The Art of Electronics*. Cambridge: Cambridge University Press.
- Hughes, M. L. (2013). *Objective Measures in Cochlear Implants*. San Diego, CA: Plural Publishing Inc.
- Hughes, M. L., Vander Werff, K. R., Brown, C. J., Abbas, P. J., Kelsay, D. M., Teagle, H. F., et al. (2001). A longitudinal study of electrode impedance, the electrically evoked compound action potential, and behavioral measures in nucleus 24 cochlear implant users. *Ear Hear.* 22, 471–486. doi: 10.1097/00003446-200112000-00004
- Khater, A. M., Moustafa, M. F., Said, A., and Fahmy, H. S. (2015). An evidence-based guide for intraoperative cochlear implant backup use. *Int. J. Pediatr. Otorhinolaryngol.* 79, 1500–1504. doi: 10.1016/j.ijporl.2015.06.037
- Mesnildrey, Q., Macherey, O., Herzog, P., and Venail, F. (2019). Impedance measures for a better understanding of the electrical stimulation of the inner ear. *J. Neural Eng.* 16:016023. doi: 10.1088/1741-2552/aaecff
- Newbold, C., Rachael, R., Rodney, M., Christie, H., Dusan, M., and Robert, S. (2010). Changes in biphasic electrode impedance with protein adsorption and cell growth. *J. Neural Eng.* 7:056011. doi: 10.1088/1741-2560/7/5/056011
- Newbold, C., Richardson, R., Huang, C. Q., Milojevic, D., Cowan, R., and Shepherd, R. (2004). An in vitro model for investigating impedance changes with cell growth and electrical stimulation: implications for cochlear implants. *J. Neural Eng.* 1, 1218–1227.
- Newbold, C., Risi, F., Hollow, R., Yusof, Y., and Dowell, R. (2015). Long-term electrode impedance changes and failure prevalence in cochlear implants. *Int. J. Audiol.* 54, 453–460. doi: 10.3109/14992027.2014.1001076
- Newbold, C., Silvana, M., Rachael, R., Peter, S., Millard, R., Robert, C., et al. (2014). Impedance changes in chronically implanted and stimulated cochlear implant electrodes. *Cochlear Implants Int.* 15, 191–199. doi: 10.1179/1754762813y.0000000050
- Ni, D., Shepherd, R. K., Seldon, H. L., Xu, S. A., Clark, G. M., and Millard, R. E. (1992). Cochlear pathology following chronic electrical stimulation of the auditory nerve. I: normal hearing kittens. *Hear. Res.* 62, 63–81. doi: 10.1016/0378-5955(92)90203-y
- Paasche, G., Bockel, F., Tasche, C., Lesinski-Schiedat, A., and Lenarz, T. (2006). Changes of postoperative impedances in cochlear implant patients: the short-term effects of modified electrode surfaces and intracochlear corticosteroids. *Otol. Neurotol.* 27, 639–647. doi: 10.1097/01.mao.0000227662.88840.61
- Saunders, E., Lawrence, C., Antje, A., William, S., Michelle, K., Mathias, S., et al. (2002). Threshold, comfortable level and impedance changes as a function of electrode-modiolar distance. *Ear Hear.* 23, 28S–40S.
- Smith, D. W., and Finley, C. C. (1997). Effects of electrode configuration on psychophysical strength-duration functions for single biphasic electrical stimuli in cats. *J. Acoust. Soc. Am.* 102, 2228–2237. doi: 10.1121/1.419636
- Tykocinski, M., Cohen, L. T., and Cowan, R. S. (2005). Measurement and analysis of access resistance and polarization impedance in cochlear implant recipients. *Otol. Neurotol.* 26, 948–956. doi: 10.1097/01.mao.0000185056.99888.f3
- Tykocinski, M., Duan, Y., Tabor, B., and Cowan, R. S. (2001). Chronic electrical stimulation of the auditory nerve using high surface area (HiQ) platinum electrodes. *Hear. Res.* 159, 53–68. doi: 10.1016/s0378-5955(01)00320-3
- Vanpoucke, F., Zarowski, A., Casselman, J., Frijns, J., and Peeters, S. (2004). The facial nerve canal: an important cochlear conduction path revealed by Clarion electrical field imaging. *Otol. Neurotol.* 25, 282–289. doi: 10.1097/00129492-200405000-00014
- Vanpoucke, F. J., Zarowski, A. J., and Peeters, S. A. (2004). Identification of the impedance model of an implanted cochlear prosthesis from intracochlear potential measurements. *IEEE Trans. Biomed. Eng.* 51, 2174–2183. doi: 10.1109/tbme.2004.836518
- von Rohr, R. (2011). *Cochlear Implant Impedance Telemetry Measurements and Model Calculations to Estimate Modiolar Currents*. Zürich: University of Zurich.
- Wieckowski, A. (1999). *Interfacial Electrochemistry: Theory, Experiment, and Applications*. Boca Raton, FL: CRC Press.
- Wolfe, J. (2017). *Cochlear Implants: Audiologic Management and Considerations for Implantable Hearing Devices*. San Diego, CA: Plural Publishing Incorporated.
- Wolfe, J., and Schafer, E. C. (2014). *Programming Cochlear Implants*. San Diego, CA: Plural Publishing.

Conflict of Interest: The authors declare that this study received equipment from Cochlear, Ltd. They were not involved in the study design, collection, analysis, interpretation of data, the writing of this article or the decision to submit it for publication.

Copyright © 2020 Di Lella, Parreño, Fernandez, Boccio and Ausili. This is an open-access article distributed under the terms of the Creative Commons Attribution License (CC BY). The use, distribution or reproduction in other forums is permitted, provided the original author(s) and the copyright owner(s) are credited and that the original publication in this journal is cited, in accordance with accepted academic practice. No use, distribution or reproduction is permitted which does not comply with these terms.